



Recommendations for Urban Planning Based on Non-motorized Travel Data and Street Comfort

Linfeng Xie, Zhiyong Yu, Fangwan Huang, and Daoye Zhu^(✉)

College of Computer and Data Science, Fuzhou University, Fuzhou 350108, China
zhudaoye@fzu.edu.cn

Abstract. Urban open spaces provides various benefits to citizens, but the thermal environment under this space is being affected by the accelerated urbanization and global warming. Based on this, this paper is dedicated to conducting research on improving the attractiveness of outdoor environmental spaces and improving outdoor thermal comfort. The main work of this paper is first to propose a street comfort model by considering both environmental and climatic factors, which is trained to learn using indirect data. Secondly, the comfort level of each street is combined with the frequency of non-motorized trips on that street to obtain the urgency index of rectification for that street and to achieve accurate recommendations for urban planning. Considering the public accessibility of the data in the paper in cities across China, this study can be easily deployed to other cities to support urban planning and provide useful recommendations for improvement of urban open spaces.

Keywords: Indirect learning · Street solar radiation value · Street comfort model · Street rectification urgency index

1 Introduction

With warming and urbanization, heat is increasing globally, especially in large cities with high population mobility. One of the biggest difficulties for future urban planning is to develop and protect cities to make them livable and sustainable. Outdoor comfort is an important evaluation indicator for urban planning as well as for architectural design. An increase in outdoor comfort is often accompanied by an increase in the number of hours residents spend outdoors, which also means an increase in urban vitality. As the research on urban climate has intensified, scholars have also paid more attention to how to create more comfortable outdoor spaces in order to improve the service efficiency of urban outdoor spaces.

Most of the studies on urban outdoor comfort have been conducted on the whole city or the whole area. However, this paper considers that after excluding parks and amusement parks, which are open-air entertainment and recreation places, the traffic axis is the largest piece of urban open spaces, so this paper locks the scope to the street level to study the comfort of streets. The work in this paper can be divided into the

following two steps: 1. Integrate both environmental and climatic factors to propose a street comfort model. 2. Combine the comfort level of each street with the frequency of non-motorized trips on that street to get the urgency index of rectification for that street and achieve accurate recommendation for urban planning.

In terms of environmental factors, this paper considers the degree of street greenery. Greenery is one of the effective means to promote the adoption of non-motorized travel activities by citizens, and exists in various forms in streets, including trees, environmental zones, and green walls. Traditional urban greenery measurement methods cannot encompass all forms of greenery and cannot accurately reflect the degree of pedestrian visibility of greenery. Therefore, this paper uses the panoramic image and semantic segmentation method of Baidu Street View (BSV) to calculate the Green View Index (GVI) with reference to the pedestrian's visual perspective to improve the comprehensiveness of the quantitative representation of street greenery. As for the climatic factors, in addition to the conventional temperature and humidity, this paper also considers the street-level solar radiation. It depicts the horizontal solar radiation of each street per hour, which can well represent the exposure of residents to sunlight. Considering that the street orientation has a significant effect on the radiation value, this paper first obtains the street orientation by road network calculation, and then adds it to the existing radiation estimation method based on street images [1] to improve the accuracy of estimating the street-level solar radiation value. Finally, the comfort value of each street is obtained by using a street comfort model by considering both environmental and climatic factors.

In urban planning, considering that both street comfort and non-motorized travel data are spatio-temporally heterogeneous and can reflect the detailed situation of each street at each time, this paper combines the comfort value of each street and the frequency of non-motorized travel of that street to obtain a reasonable street rectification urgency index. Finally, using the ranking of this index and combining detailed research and discussion analysis, we propose targeted suggestions for the rectification of existing roads in the city.

2 Related Work

2.1 Estimation of Street Solar Radiation Values

For the calculation of street solar radiation values, the two main traditional methods are inversion by remotely sensed data and calculation by digital urban models. Different metrics such as canopy cover and vegetation index can be calculated from remotely sensed images to indicate the microclimate regulation of urban vegetation [2] and added to the estimation of solar radiation at ground level. However, it is difficult to simulate the solar radiation reaching the ground with only the remote sensing data overhead. This is because the vertical structure of the street canopy and other urban features under the street canopy affect the solar radiation within the street, which are not reflected in the high-view remote sensing data [3]. On the other hand, with the advent of high-resolution digital city models, it is possible to simulate the transmission of solar radiation within the streets. However, most digital city models oversimplify the complex geometry within the city streets [4]. Recently, street view images provided by online maps such as Google Maps, Baidu Maps, Tencent Maps, and Mapillary have provided a novel and low-cost

data source for urban studies. These street view image data enable a more comprehensive description of high-density street patterns to address the shortcomings of the two traditional methods mentioned above. This computational approach first originated from the thermal comfort model proposed by RayMan [5] in 2007, who converted the manually taken streetscape photos into Sky View Factor (SVF) and then added the calculation of horizontal street radiation. Since then, with the development of deep learning technology and the opening of street view images on the Internet, more studies based on this idea have started to study the distribution of street level radiation throughout the city [1, 6] and use it to make suggestions for urban planning. In this paper, borrowing from Deng Mingyu et al.'s method [7], we use deep learning techniques to process Baidu street view images so as to derive the sky visibility, and then use this parameter to estimate the solar radiation at street level, while the innovation is to include the preprocessing of street direction in the calculation process.

2.2 Comfort Model

Currently available comfort models use two main types of objective elements: local climatic factors and urban environmental parameters. Unfortunately, the existing models model only one of these categories and do not consider both at the same time. For example, the Physiological Equivalent Temperature (PET) [8], the Predicted Mean Vote (PMV) [9], the Universal Thermal Climate Index (UTCI) [10] and Standard Effective Temperature (SET) [11] are the four most commonly used comfort assessment models [12], all of which use only climatic factors in the objective elements part. While studies by Mohammad Fahmy [13] and Hongxuan Zhou [14] et al. used only urban environmental parameters.

For traditional modeling of comfort models, there are mainly empirical modeling based on theoretical knowledge and traditional supervised learning methods, which often require large costs to acquire data. For example, the fully connected neural network model used by Dyvia [15] and the K-Nearest Neighbor (KNN) used by Lei Xiong [16] are trained based on known PMV values. However, the comfort model proposed in this paper is characterized by parameter diversity, and if supervised learning is used, a large number of questionnaire research results are required to label the data, which is time-consuming and labor-intensive. In order to solve the above problems, this paper proposes to construct a complete closed network model based on indirect data first, and then extract the intrinsic relationship between street environment factors and street comfort through the overall model, so that the comfort model to be constructed can be obtained.

3 Method

The purpose of this paper is to construct a street comfort model that considers both environment and climate, and to combine it with street pedestrian flow to generate street rectification urgency indicators to provide reliable suggestions for urban planning and rectification. The methodological framework of this study is shown in Fig. 1 and consists of three main stages. In the first stage, SVF and GVI are first estimated from Baidu Street View panoramic images, and then SVF is combined with street direction, sun path and extraterrestrial solar radiation to calculate street-level solar radiation values. In the second stage, a neural network is constructed based on indirect learning with environmental factors, climate factors, and non-motorized travel data as inputs, from which a comfort model is extracted. In the third stage, a set of streets with low comfort level and high pedestrian traffic is obtained by constructing a street rectification urgency index and fed back to the city planning department.

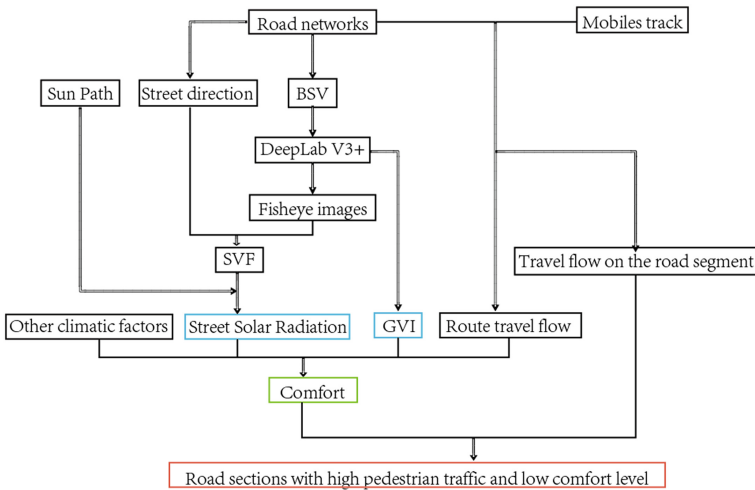


Fig. 1. Research framework for urban planning recommendations based on non-motorized travel data and street comfort.

3.1 Estimation of Street Solar Radiation Values Based on Baidu Street View Map

In this section, the method of using BSV images to estimate the street solar radiation values will be described. It consists of three main parts: (1) generating fisheye images from BSV panoramic images and calculating SVF, (2) obtaining solar irradiation from sun path map and fisheye images, and (3) estimating street solar radiation values.

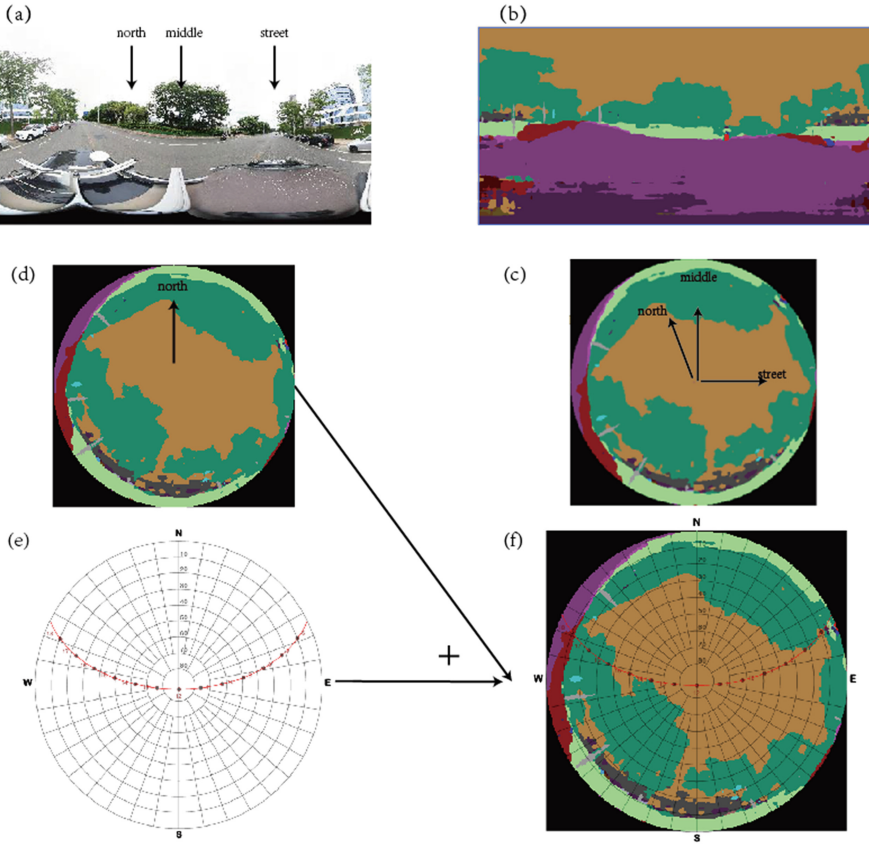


Fig. 2. Flow of calculating solar radiation of a street using BSV image with sampling point (119.2845351, 26.0041302) as an example. (a) panoramic image obtained using Baidu Map API; (b) panoramic map obtained by DeepLab V3+; (c) fisheye map converted from the panoramic map; (d) fisheye map obtained by considering the street direction and rotating figure (c) to face upward in the due north direction; (e) sun path map of 2017-6-15; (f) fisheye map (d) with the street direction considered and the sun path diagram (e) superimposed on the diagram.

3.1.1 Generate Fisheye Images from BSV Panoramic Images and Calculate Sky Visibility

In real roads, the solar radiation values reaching the ground are influenced by shading such as buildings and trees. The traditional way to calculate radiation is to use remote sensing data or urban modeling to estimate it, but both of them use top-down calculation, which does not describe the shading of trees and buildings in the street well. Based on this, this paper proposes to use a bottom-up approach to calculate solar radiation values.

The SVF measures the proportion of the sky seen at a location in the street; a smaller SVF means more occlusion at that location point, and vice versa means less occlusion. Using fisheye images to calculate the SVF is more in line with the real street view [7]. Taking Fig. 2 as an example, the specific approach is as follows: (1) the panoramic

image of Fig. 2(a) is obtained using Baidu Map API; (2) the extraction of street elements such as trees, green, sky, and buildings is completed by DeepLab V3+ model [17], as shown in Fig. 2(b), where orange represents the sky, black represents the background, and green, red, etc. represent other street elements; (3) according to the method proposed by XiaoJiang Li [6], the panoramic image is converted into a fisheye image, as shown in Fig. 2(c); (4) SVF can be expressed by the percentage of pixels representing the sky in the fisheye image, and the calculation equation is as follows.

$$\text{SVF} = \frac{\text{number of sky pixels}}{\text{number of total pixels} - \text{number of background pixels}} \quad (1)$$

3.1.2 Acquisition of Solar Irradiation from Sun Path and Fisheye Images

Street alignment affects the timing of exposure to direct sunlight. In north-south oriented streets, the street surface will be exposed to direct sunlight near noon, but will be influenced by shading at other times. However, in east-west oriented streets, it is more likely to be exposed to direct sunlight all day from morning to afternoon [1]. In order to reduce the effect of street orientation, the literature [6] proposes to rotate the fisheye map so that it has the same coordinate system as the sun path map. This method uses the Google Street View (GSV) panoramic image because Google Maps has an interface to provide the return street orientation. However, the coverage of GSV panoramic image for Chinese road network is seriously insufficient, so this paper uses BSV panoramic image, which has significantly higher coverage than GSV panoramic image, see Fig. 3 for details. Unfortunately, Baidu map does not provide the street direction data, so this paper proposes a processing method to obtain the street direction.

First, sampling points are generated on the road network at 50 m equal intervals, as shown in Fig. 4(a). Then the road network is segmented with these sampling points on the arcgis software, and a road section is generated between every two adjacent sampling points, followed by the direction line of the road section, as shown in Fig. 4(b), from which the street orientation θ° can be obtained. The clockwise deflection θ° in the due north direction is the direction of the street where it is located. Finally, the fisheye image in Fig. 2(c) is rotated by $(450^\circ - \theta^\circ) \% 360^\circ$ (“%” means taking the remainder) to obtain Fig. 2(d). The rotated fisheye image will have the same coordinate system as the sun path map.

The sun path map is generated by Rayman software [5] after inputting the position and date, as shown in Fig. 2(e), where the points in the map represent the position of the sun at a given moment. Finally, overlaying the sun path diagram with a fisheye diagram considering the street direction yields Fig. 2(f), so that the sun exposure at each moment (i.e., whether the sun is blocked or not) can finally be determined.



Fig. 3. Coverage of panoramic images in Google Maps and Baidu Maps. (a) Google Maps, the locations marked with circles represent the presence of panoramic images; (b) Baidu Maps, the road sections marked with dark blue represent the presence of panoramic images.

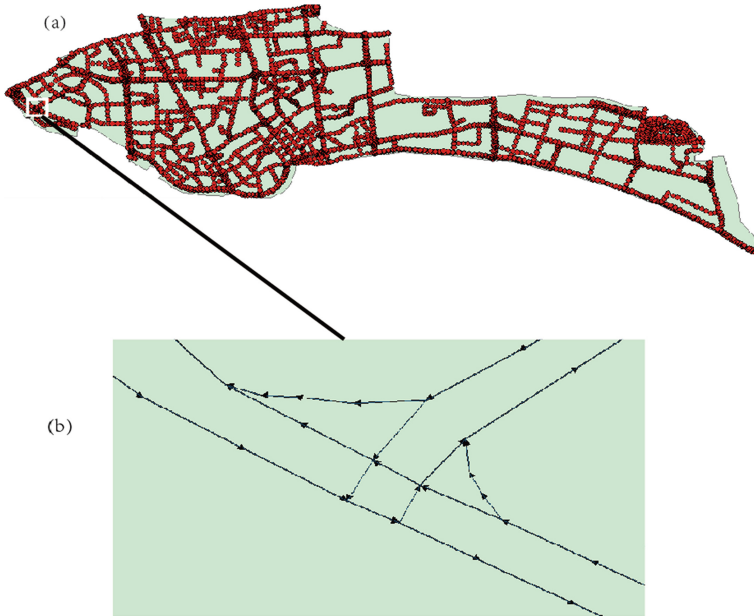


Fig. 4. Street directions (a) Sampling points generated along a street; (b) Street directions generated by a subregion based on a road segment.

3.1.3 Estimated Street Solar Radiation Values

Solar radiation in the transmission process can be divided into direct radiation, reflected radiation and diffuse radiation. Since the reflected radiation accounts for a very small proportion of the total radiation, the total radiation (G_{street}) is often equivalent to the sum of direct radiation (I_{street}) and diffuse radiation (D_{street}) [7], as shown in Eq. (2).

$$G_{street} = I_{street} + D_{street} \tag{2}$$

The formula for calculating I_{street} is as follows.

$$I_{street} = I_{open} * f \quad (3)$$

I_{open} is the direct radiation under the free field of view, the calculation method can be found in the literature [1]; f is a binary variable, as shown in Fig. 2(f), if a point belonging to a moment in the sun path diagram is in the region where the sky is located (i.e., the moment point is in the orange region), it represents not blocked by obstacles, at this time the value is 1, anyway, it is 0.

The formula for calculating D_{street} is as follows.

$$D_{street} = D_{iso_open} * \psi_{sky} + D_{aniso_open} * f + D_{cloud_open} * \psi_{sky} \quad (4)$$

D_{iso_open} is the isotropic diffuse radiation on the horizontal surface in the free horizon; D_{aniso_open} is the anisotropic diffuse radiation on the horizontal surface in the free horizon, which tends to concentrate near the Sun and is distinguished according to whether the Sun is directly visible or not; D_{cloud_open} is the diffuse radiation on the horizontal surface in the free horizon due to cloud cover; The calculation of the above three can be found in the literature [1]. ψ_{sky} is the SVF, and the specific calculation procedure is described in Subsect. 3.1.1; The description of f is detailed in Eq. (3).

3.2 Model for Calculating GVI

Urban greening will provide a variety of benefits to citizens, including physical, environmental and social benefits, thus promoting urban livability and vitality [19] and making urban open spaces more attractive. Among them, the impact of street greening on comfort is mainly reflected in two aspects: 1. Street greening, as an important part of street spaces planning and design, has been proven by numerous studies to be an important way to improve the thermal comfort of street spaces [20]. Therefore, it is important to investigate the mechanism of the effect of street greening on outdoor comfort to better utilize street planting design to improve pedestrian thermal comfort. 2. Studies have shown that residents' exposure to natural and semi-natural environments, whether long-term or short-term, can have certain benefits on physical and mental health [21]. A Japanese study analyzed the 5-year survival rate of 3144 elderly people and concluded that walkable urban green spaces have a positive impact on extending the life expectancy of urban elderly [22]. In addition to physical health benefits, urban greenery can also provide a sense of social support to residents. by measuring social contact and health status of 10,089 residents in the Netherlands, Maas et al. found that a large number of outdoor green spaces can reduce loneliness [23], as well as enhance the quality of life and well-being of residents [24, 25].

GVI is the proportion of greenery visible from a given location. In this paper, GVI will be used to quantify street greenery. Since GVI is mainly for green vegetation within the visual range of pedestrians on the street, and the top and bottom of the panoramic image also have more serious distortion, it is necessary to set the range of the visual fence and keep the middle part of the image with less distortion. In this paper, the method of Yin et al. [2] is adopted, and the part of the panoramic image corresponding to the pedestrian view with less distortion is cropped and utilized, as shown in Fig. 5.

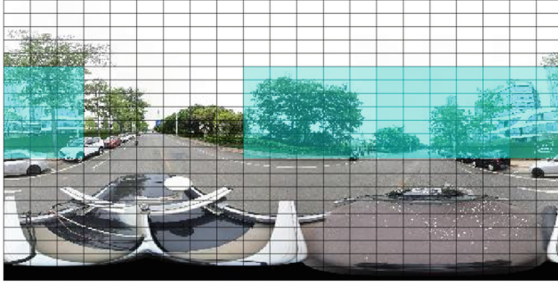


Fig. 5. A figure caption is always placed below the illustration. Short captions are centered, while long ones are justified. The macro button chooses the correct format automatically.

The GVI can be calculated by Eq. (5), and the total number of pixels and the number of green pixels are for the blue area in Fig. 5. The GVI of the sampled points is calculated and then correlated to the road of the area where they are located, and the GVI distribution of the whole area can be obtained, as shown in Fig. 6.

$$\text{GVI} = \frac{\text{number of green pixels}}{\text{number of total pixels}} \quad (5)$$

gvi_value
 — 0.028416 - 0.314269
 — 0.314270 - 0.438188
 — 0.438189 - 0.553452
 — 0.553453 - 0.684996
 — 0.684997 - 0.996208



Fig. 6. GVI distribution of the whole region.

3.3 Indirect Learning Based Comfort Model Construction

Traditional outdoor comfort models mainly focus on thermal comfort as well as visual comfort, but less consider these two together. Based on this, this paper proposes a neural network model based on indirect learning to construct a new comfort model. First, the constructed comfort model considers both visual and thermal comfort factors, and concentrates on the street level, which is finer in granularity than previous work. Second, unlike previous supervised learning methods or empirical modeling based on theoretical knowledge, the comfort model proposed in this paper uses indirect learning to extract the intrinsic relationship between street environment factors and street comfort. This approach was mainly used in cases where experimental results require large computational costs or where experimental results are more difficult to obtain [26]. Given the very high cost and operational difficulty of obtaining street comfort by means of questionnaires, this paper adopts an indirect learning-based approach to construct a street comfort model. This is done by treating the street comfort model as a sub-network of the overall model, and the overall model is obtained using supervised learning. When the training of the overall model is completed, it can be approximated that its sub-network has also completed training.

In this section, the closed-form solution of the comfort model will be illustrated, discussing the overall model construction process. First of all, it is necessary to explain that residents receive two main factors for travel, which are subjective travel purpose and objective external factors. The subjective travel purpose can be reflected in the individual's travel intentions or in the trajectory data by the routes connected to the origin and destination points. For example, trips to work are generally not affected by personal travel intentions and usually have an inherent travel route from home to work, while trips for leisure purposes such as walking and exercising are more affected by personal travel intentions and usually have a route from the leisure place to other locations. Thus, this paper considers that travel trajectories with the same origin and destination points have the same travel purpose. The objective external factors are considered as climate factors and street environment factors.

Since the final travel data will be influenced by both subjective and objective factors, and the comfort model proposed in this paper is only influenced by objective factors, the influence of subjective factors needs to be quantified in the process. From the description in the previous paragraph, it can be seen that the subjective factors can be quantified by the origin and destination points, i.e., the influence of subjective factors can be considered fixed under the premise of having the same origin and destination points or the same travel routes. From this, two data features can be further elicited, the length of the travel route and y_{ideal} . y_{ideal} represents the ideal number of people traveling under a particular travel route. For y_{ideal} , it can be understood that the ideal value of the number of travelers on a certain route, under the condition that the external environment is all in ideal conditions, should satisfy $y_{ideal} \geq y_{realty}$, y_{realty} is the actual number of travelers on a certain route at a certain moment. Given that y_{realty} is unavailable data, the maximum value of $\max(y_{realty})$ will be used as an approximation of y_{ideal} in the subsequent study of this paper.

In summary, this paper proposes a solution that allows the measurement of the relationship between street environmental factors and street comfort ontology and is represented as a neural network, as shown in Fig. 7. The overall model of the solution is constructed by the two modules F1 and F2 together. One of the modules, F1, is the comfort model to be constructed in this paper, and its output node values are the comfort values. As mentioned in the previous paragraph, residents' trips are mainly influenced by subjective trip purpose y_{ideal} and objective external factors, while the F2 module constructs the relationship between these data features in the form of a neural network. The y_{realty} is a quantitative representation of the residents' travel data; the weeks represent the weeks of the year, expressing the temporal order of the input data; the path length represents the length of a travel route.

Although the purpose of this paper is to construct a comfort model, the participation of the real values of comfort is not required in the model training process, but the comfort model is obtained indirectly by learning from the other data features mentioned above. In this paper, we first perform supervised learning of the overall model, with the six objective factor features in the F1 model and the three features y_{ideal} , weeks and path length in the F2 module as input features, and y_{realty} as output features. Wait for the overall model training to converge before extracting the weights of the F1 module, and use the network model of the F1 module as the final comfort model.

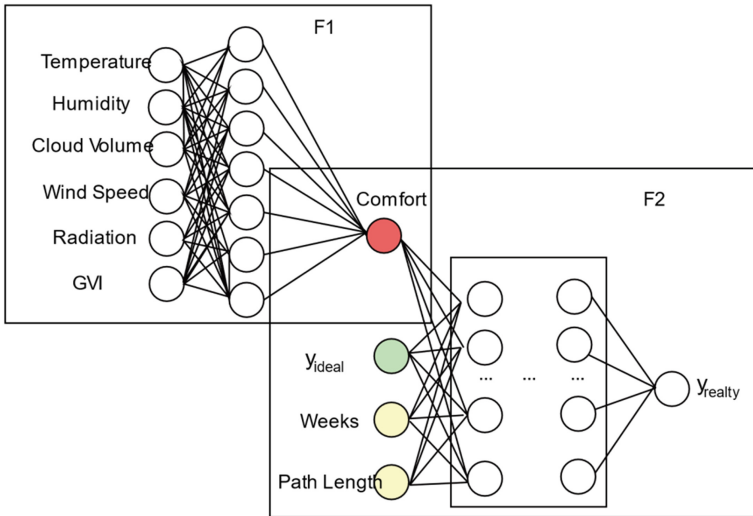


Fig. 7. Overall model including comfort model.

3.4 Methodology for Estimating Street Correction Urgency Indicators

The purpose of calculating the street correction urgency indicator is to identify a set of road sections with high pedestrian flow and low comfort level, and to provide targeted suggestions for the street component of urban planning. For this indicator, two main factors are considered, count and comfort, where count is obtained statistically and refers to the pedestrian flow of a road section over a certain period of time, and comfort is calculated by the comfort model constructed in Subsect. 3.3. Since the range of values of the two results for count and comfort may be very different, the two features are first normalized in this paper. Then each is classified into 5 levels according to the values, as shown in Eq. (6). The final street improvement urgency index is obtained by multiplying the ranks of these two features, as shown in Eq. (7). Urgency is larger to indicate that the street improvement is more urgent.

$$F(x) = \begin{cases} 1, & \text{MinmaxScaler}(x) \in [0, 0.2) \\ 2, & \text{MinmaxScaler}(x) \in [0.2, 0.4) \\ 3, & \text{MinmaxScaler}(x) \in [0.4, 0.6) \\ 4, & \text{MinmaxScaler}(x) \in [0.6, 0.8) \\ 5, & \text{MinmaxScaler}(x) \in [0.8, 1] \end{cases} \quad (6)$$

where $\text{MinmaxScaler}(\cdot)$ is the normalization function.

$$\text{urgency} = F(\text{comfort}) * F(\text{count}) \quad (7)$$

4 Experimental Design and Results Analysis

4.1 Experimental Design

4.1.1 Study Area

In this paper, relevant experiments were conducted in Taijiang District, Fuzhou City, Fujian Province. Fuzhou City is located in the eastern part of Fujian Province and has a typical subtropical monsoon climate. According to the Statistical Bulletin of National Economic and Social Development of Fuzhou City in 2021, the resident population of Fuzhou is 8.42 million. As a typical representative city with hot summers and warm winters, Fuzhou has an annual average of 32.6 days of high temperature in the past 30 years, and has been crowned as the “top furnace city”. According to the data provided by Fujian Meteorological Bulletin, Fujian Province experienced 13 high temperature processes in 2020, with the highest extreme temperature in the province occurring in Fuzhou City [27]. The large resident population and the hot climate factors make Fuzhou city a suitable area for this paper to study summer comfort.



Fig. 8. Location and map of the study area (a) Location of the main urban areas in Fuzhou City, the area marked in green is the Taijiang District to be studied in this paper. (b) Sampling points generated along the streets with 50 m interval, total 5361 points.

4.1.2 Data Collection

The datasets used in this paper include (1) Fuzhou city street vector map, as shown in Fig. 8(a), from OpenStreetMap (<https://www.openstreetmap.org>). (2) Hourly meteorological data from June 2017 to September 2017, including temperature, humidity, wind speed, and cloudiness, from World Weather (<https://rp5.ru/>). (3) Hourly total solar radiation as well as direct radiation in Fuzhou City from June 2017 to September 2017 were obtained from the Xiehe Energy Platform (<https://www.xihe-energy.com/>). (4) Solar zenith angle and extraterrestrial radiation data. They can be obtained by entering the location, time zone, and date in the interface provided by the National Renewable Energy Laboratory (<https://midcdmz.nrel.gov/solpos/solpos.html>). (5) Trajectory data of pedestrians traveling with Mobiles, provided by the Fuzhou Municipal Bureau of Transportation. (6) Panoramic image of Baidu street view.

The BSV panoramic image is acquired in two steps: (1) Generate sampling points along the street with an average sampling distance of about 50 m, as shown in Fig. 8(b). (2) The BSV panoramic images of each sampling point are acquired using the API interface provided by Baidu Maps (<https://lbsyun.baidu.com/index.php?title=viewstatic>). Finally, 5361 valid street panoramas were obtained.

4.2 Experimental Results

4.2.1 Validation of the Effect of Street Direction Treatment

Buildings and trees along the street can block the sun's rays. The sun rises in the east and sets in the west, so this phenomenon is especially obvious for streets running north-south, while streets running east-west are less affected by this phenomenon, so the street orientation is a factor that cannot be ignored when calculating solar radiation at the street

level. This section will verify the validity of the street orientation treatment proposed in Subsect. 3.1.2.

Figure 9 shows the data for location point 5 in Fig. 10, which is located on a street that runs east-west and has a dormitory building on one side of the road. From Fig. 9(c), it can be seen that the estimated solar radiation before 8 o'clock is significantly lower when street direction processing is not added. The reason for this is that if the solar radiation value is estimated directly from the fisheye map obtained from the Baidu Map street view image (i.e., Fig. 9(a)), the solar radiation before 8:00 is considered to be blocked by buildings. However, the street actually runs east-west and the sunlight is not blocked in the morning. Figure 9(b) shows the fisheye diagram generated by adding the street orientation processing, from which the estimated solar radiation is obtained as shown in the orange curve in Fig. 9(c). It is clear that the orange curve can better fit the true value of solar radiation during the 6:00–9:00 h.

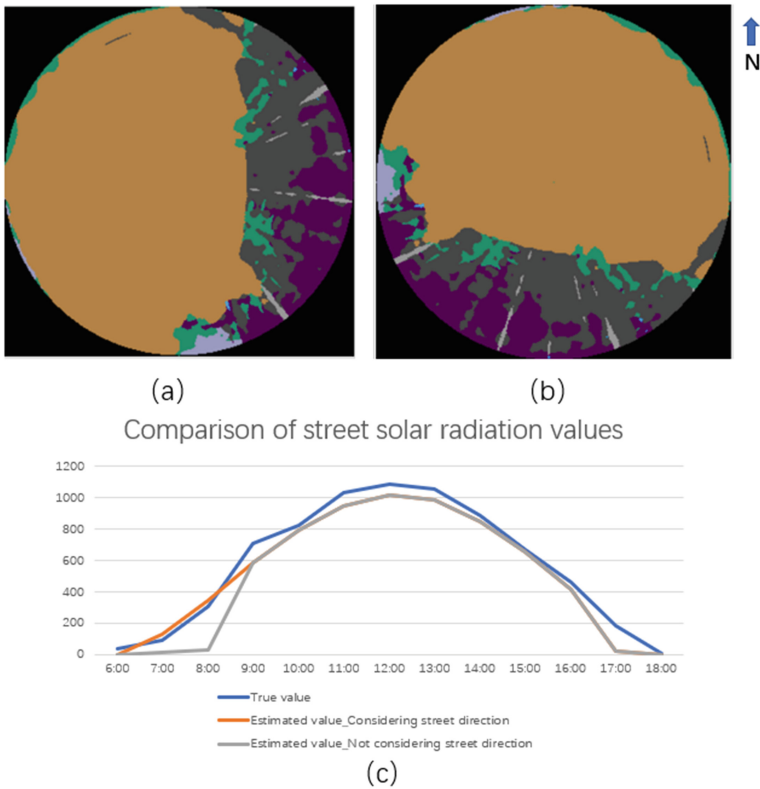


Fig. 9. Street direction (a) Fisheye map obtained by direct processing from Baidu Map Street View image without additional consideration of street direction; (b) Fisheye map obtained by additional processing with street direction on top of Baidu Map Street View image; (c) Comparison of street-level solar radiation values. (Color figure online)

4.2.2 Performance Evaluation of Methods for Estimating Solar Radiation Values in Streets

In this section, the BSV-based solar radiation estimation method will be evaluated using data measured in the field. The authors measured the real data of street solar radiation with solar radiation detection instruments on the campus of Fuzhou University on two days, 2022.07.26 and 2022.07.30. Due to the problem of rainfall, radiation data were not collected for the intermediate days. The measurement location points are shown in Fig. 10(a), there are 6 location points, and each location corresponds to the measurement reality as shown in Fig. 10(b). The following two factors are taken into consideration when selecting the location points: the street direction and the blockage of solar radiation by the buildings beside the road. As shown in Fig. 10(a), location 2, 4, and 6 are located in the north-south direction, and trees are planted on both sides of location 2 and 4, which will block the sunlight in the morning or evening. The trees on the right side of location



Fig. 10. Live map of the measurement sites located on the Fuzhou University campus. (a) Location of the measurement site on the map; (b) live street view of the corresponding location point; (c) live street view of location point 1 in 2019; (d) live street view of location point 1 in 2022.

6 and the dormitory building on the left side also block the sunlight in the morning and evening. Locations 1, 3, and 5 are located in the east-west direction, but location 1 has a thicker tree shade, location 3 has almost no shade, and there is a dormitory building on the side of location 5.

Figures 11 and 12 show the differences between the real and estimated values of street solar radiation for two days, 2022.07.26 and 2022.07.30, respectively. From the figures, it can be seen that the estimated street radiation values at locations 3 and 5 can fit the true values well. The true values of position 4 at 9:00 and position 5 at 10:00 in Fig. 11 are significantly lower than the estimated values, which may be caused by the sudden passing of clouds in the sky. The deviation between the estimated and true values of location 1, 2 and location 6 at 14:00 may be due to the fact that the street view image in Baidu Maps was updated in 2019, and the trees have grown during these years, thus blocking more sunlight and reducing direct radiation, which in turn causes the true value of radiation to be lower than the estimated value at some times. Taking location 1 as an example, Fig. 10(c) and Fig. 10(d) represent the actual road map of location 1 in 2019 and 2022 respectively, and it can be clearly seen that the trees on both sides of the road in 2022 have grown very densely compared to the road condition in 2019, leaving only a small gap for direct sunlight to pass through.

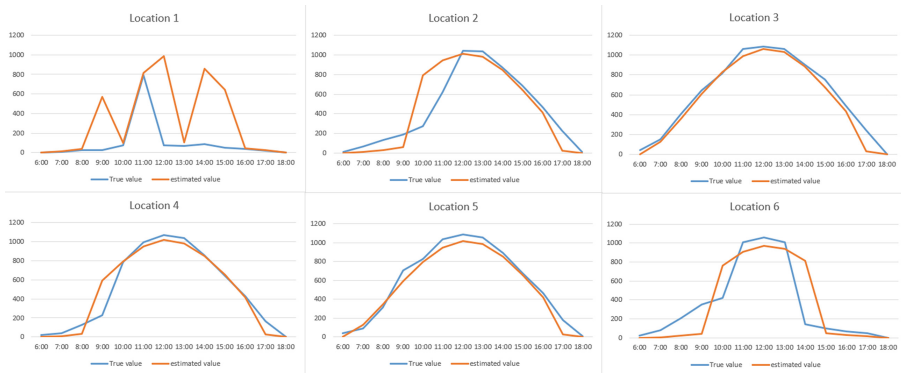


Fig. 11. 2022.07.26 Comparison plot of the real and BSV-based solar radiation estimates of street solar radiation detected at measurement sites located on the Fuzhou University campus.

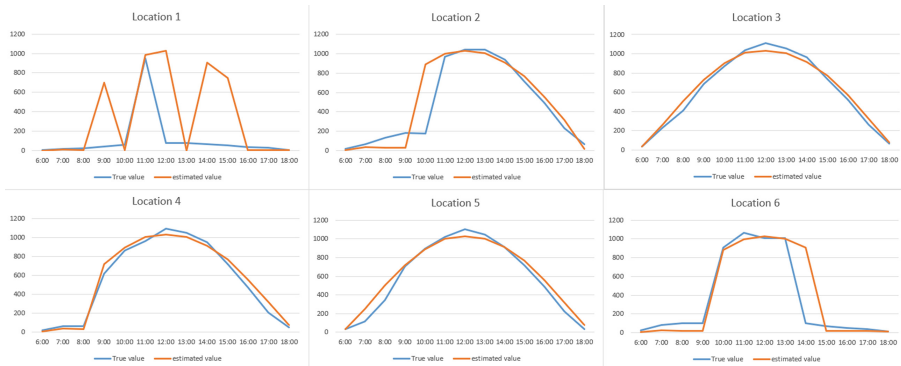


Fig. 12. 2022.07.30 Comparison plot of the true and BSV-based solar radiation estimates of street solar radiation detected at measurement sites located on the Fuzhou University campus.

4.2.3 Constructing a Comfort Model Based on Indirect Data for Performance Evaluation

Since the proposed multiparameter comfort model in this paper lacks labels for supervised learning and performance evaluation, this section will demonstrate the effectiveness of the multiparameter comfort model by verifying the feasibility of the method of constructing a comfort model based on indirect learning. Based on the fact that most outdoor comfort models refer specifically to thermal comfort models, this paper will first construct the conventional thermal comfort model (shown in Fig. 13) through indirect learning and compare its performance with the supervised model proposed by Dyvia.

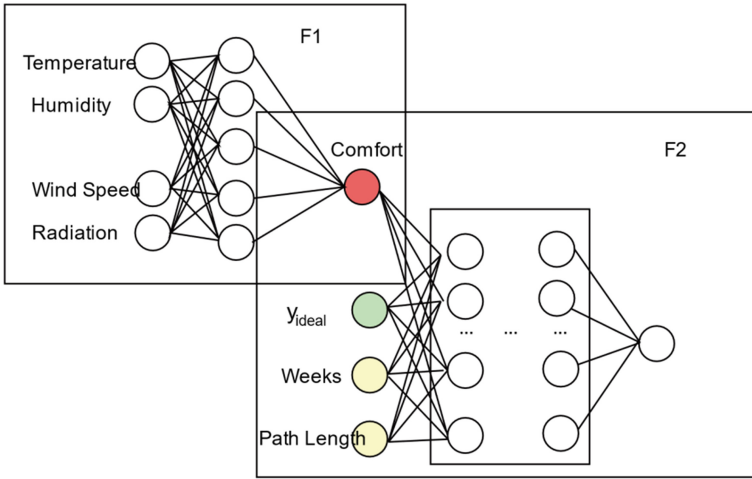


Fig. 13. Construction of thermal comfort model based on indirect learning.

The evaluation indexes used in this paper include: Mean Absolute Percentage Error (MAPE), Mean Absolute Error (MAE) and Root Mean Square Error (RMSE), which are calculated as follows.

$$\text{MAPE} = \frac{100\%}{N} \sum_{i=1}^N \left| \frac{\tilde{y}_i - y_i}{y_i} \right| \quad (8)$$

$$\text{MAE} = \frac{1}{N} \sum_{i=1}^N |\tilde{y}_i - y_i| \quad (9)$$

$$\text{RMSE} = \sqrt{\frac{1}{N} \sum_{i=1}^N (y_i - \tilde{y}_i)^2} \quad (10)$$

where N denotes the number of data sets, \tilde{y}_i denotes the estimated value of the model, y_i denotes the true value, and \bar{y}_i is the mean value of $N y_i$. All the above three indicators are as small as possible. The PMV value was obtained according to the PMV model

proposed by Professor P.O. Fanger from Denmark. The PMV value is an evaluation index characterizing the human thermal response (hot and cold sensation) and represents the average hot and cold sensation of most people in the same environment. This index takes into account six factors such as human activity level, clothing thermal resistance, air temperature, air humidity, average radiation temperature, and air flow rate, etc. Rayman et al. [5] developed a software for calculating PMV values based on this, which will also be used in this paper. When processing the input data, this paper fixes the values affected by individual factors to ensure that the generated PMV values are only affected by four external environmental factors: temperature, humidity, wind speed, and radiation. The final 122 data were generated, containing 61 PMV values at 8:00 am for each day from June to July 2017 and 61 PMV values at 14:00 pm for each day from June to July 2017.

It should be noted that since the comfort value and pedestrian flow are treated in a graded manner during the subsequent calculation of the street rectification urgency index, the evaluation requirement of the comfort model in this paper is to ensure that the comfort value is on the correct grade. Based on this, both \tilde{y}_i and y_i are normalized and graded in this paper before calculating the three evaluation indexes mentioned above. The experimental results are shown in Table 1. It is easy to find that although there is a certain gap between the estimated values of the comfort model constructed based on indirect learning and the estimated values of the model constructed by the supervised learning method, the gap is within an acceptable range. The supervised learning-based network model has real PMV values as labels for network training, while the indirect learning-based network model does not have PMV values as labels, so it is normal for the supervised learning-based method to outperform the indirect learning-based method. Given the small difference in the evaluation metrics calculated by the two models, it shows the feasibility of the indirect learning-based approach to constructing the comfort model.

Table 1. Comparison of model estimates with PMV values.

Contrast Model	MAPE	MAE	RMSE
Thermal comfort model constructed based on indirect learning	20.6844	0.4475	0.7114
Thermal comfort model constructed based on supervised learning	12.7951	0.2508	0.5182

4.2.4 Validation of the Effectiveness of Street Correction Urgency Indicators

The road network in Taijiang District, Fuzhou City, is divided at 50 m intervals to obtain 1962 road sections, and then the score of each road section is calculated according to the calculation of the street improvement urgency index in Sect. 3.4. The top 100 road sections are first taken, marked in red and visualized in the road network to obtain Fig. 14(b). Figure 14(a) shows the distribution of pedestrian flow on the street, the darker the color of the road section means the higher the pedestrian flow, and several road sections with particularly high pedestrian flow also show obvious red color in

Fig. 14(b), indicating that the high value of the urgency of improvement index of these road sections is mainly caused by the abnormally high pedestrian flow.

After excluding the above-mentioned high-traffic streets, five locations were randomly selected, as shown in Fig. 14(b), and it can be seen that these locations are characterized by less vegetation on both sides and wider roads. From the left side to the right side of the map, the five locations have office buildings, intersections, Wuyi Square, schools, and Wanda Square next to each other, and the pedestrian flow in these locations is obviously larger than that in other unusual streets. This result proves that the calculation of the street improvement urgency index is reasonable.

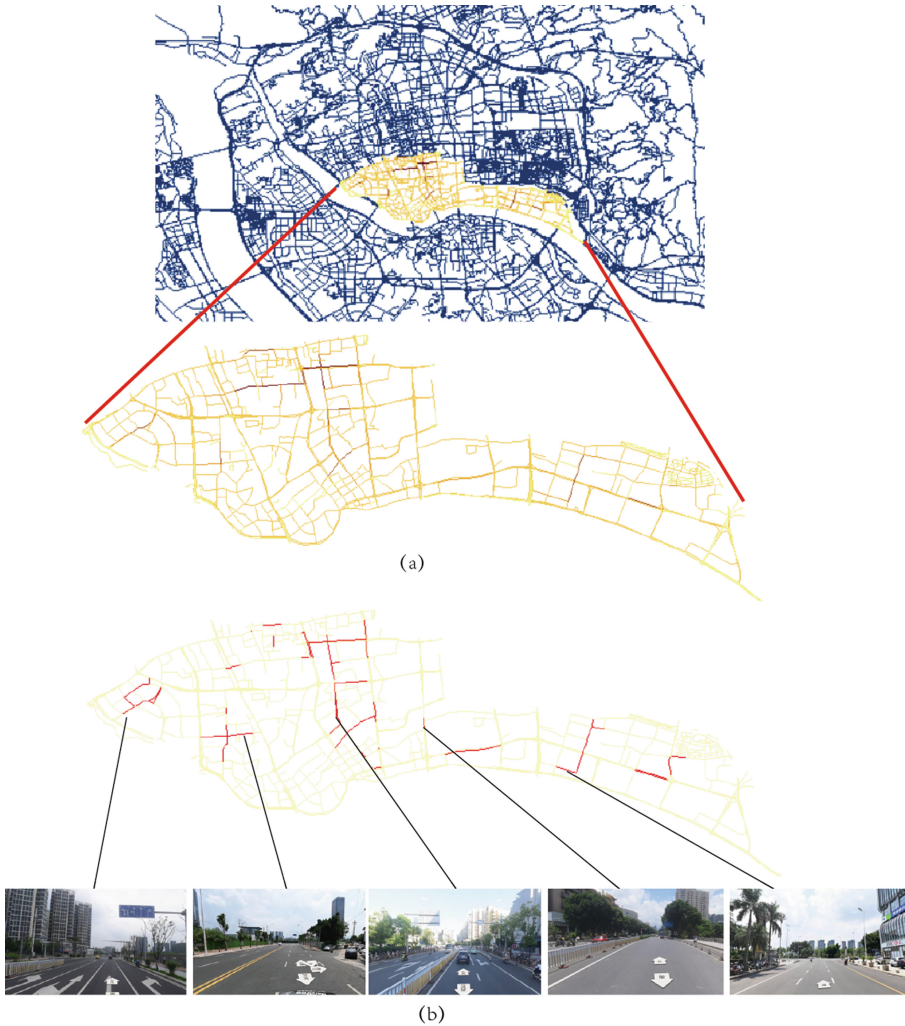


Fig. 14. (a) Street traffic distribution map. (b) Visualization of street rectification urgency indicators.

5 Summary

This paper develops a computational framework for constructing an outdoor comfort model and depicting the urgency indicators of street rectification. The framework has several advantages: (1) The construction of the street comfort model is based on indirect data for modeling, which can well solve the problems of difficulty in obtaining comfort values and high cost of obtaining them. (2) The street comfort model takes into account both visual and environmental factors and is more comprehensive. (3) In terms of environmental factors, street-level solar radiation, a weather data, is used to capture the dynamic changes of urban streets in a more fine-grained manner. (4) The street-level solar radiation is made more accurate by adding the processing of street direction in the estimation of street-level solar radiation based on BSV. (5) The proposed street rectification urgency index can reveal the road sections with high pedestrian flow and low street comfort, which facilitates urban planning. The accuracy and validity of the method are verified by taking Taijiang District, Fuzhou, China, as an example.

The public nature of the data in this paper and the proposed low-cost and efficient modeling approach make it applicable to other cities. At the same time, the generated data and maps provide a useful dataset for understanding complex urban systems.

References

1. Gong, F.-Y., Zeng, Z.-C., Ng, E., Norford, L.K.: Spatiotemporal patterns of street-level solar radiation estimated using Google Street View in a high-density urban environment. *Build. Environ.* **148** (2019)
2. Kong, F., Yin, H., Wang, C., Cavan, G., James, P.: A satellite image-based analysis of factors contributing to the green-space cool island intensity on a city scale. *Urban For. Urban Green.* **13**(4), 846–853 (2014a)
3. Li, X., Ratti, C., Seiferling, I.: Quantifying the shade provision of street trees in urban landscape: a case study in Boston, USA, using Google Street View. *Landsc. Urban Plan.* **169**, 81–91 (2018)
4. Carrasco-Hernandez, R., Smedley, A.R., Webb, A.R.: Using urban canyon geometries obtained from Google Street View for atmospheric studies: potential applications in the calculation of street level total shortwave irradiances. *Energy Build.* **86**, 340–348 (2015)
5. Matzarakis, A., Rutz, F., Mayer, H.: Modelling radiation fluxes in simple and complex environments: basics of the RayMan model. *Int. J. Biometeorol.* **54**(2) (2010)
6. Li, X., Ratti, C.: Mapping the spatio-temporal distribution of solar radiation within street canyons of Boston using Google Street View panoramas and building height model. *Landsc. Urban Plan.* **191**(C) (2019)
7. Deng M., Yang, W., Chen, C., Wu, Z., Liu, Y., Xiang, C.: Street-level solar radiation mapping and patterns profiling using Baidu Street View images. *Sustain. Cities Soc.* **75** (2021)
8. Höppe, P.: The physiological equivalent temperature – a universal index for the biometeorological assessment of the thermal environment. *Int. J. Biometeorol.* **43**, 71–75 (1999)
9. Fanger, P.O.: *Thermal Comfort*. McGraw Hill, New York (1970)
10. Jendritzky, G., de Dear, R., Havenith, G.: UTCI—why another thermal index? *Int. J. Biometeorol.* **56**, 421–428 (2012)
11. Gagge, A.P., Fobelets, A.P., Berglund, L.G.: A standard predictive index of human response to the thermal environment. *ASHRAE Trans.* **92** (1986)

12. Lai, D., et al.: A comprehensive review of thermal comfort studies in urban open spaces. *Sci. Total Environ.* **742** (2020), prepublsh)
13. Fahmy, M., Kamel, H., Mokhtar, H., et al.: On the development and optimization of an urban design comfort model (UDCM) on a passive solar basis at mid-latitude sites. *Climate* **7**(1), 1 (2019)
14. 周宏轩, 陶贵鑫, 炎欣焯, 等.: 绿量的城市热环境效应研究现状与展望. *Yingyong Shengtai Xuebao* **31**(8) (2020). (in Chinese)
15. Dyvia, H.A., Arif, C.: Analysis of thermal comfort with predicted mean vote (PMV) index using artificial neural network. In: *IOP Conference Series: Earth and Environmental Science*, vol. 622, no. 1, p. 012019. IOP Publishing (2021)
16. Xiong, L., Yao, Y.: Study on an adaptive thermal comfort model with K-nearest-neighbors (KNN) algorithm. *Build. Environ.* **202**, 108026 (2021)
17. Chen, L.-C., Zhu, Y., Papandreou, G., Schroff, F., Adam, H.: Encoder-decoder with atrous separable convolution for semantic image segmentation. In: Ferrari, V., Hebert, M., Sminchisescu, C., Weiss, Y. (eds.) *ECCV 2018*. LNCS, vol. 11211, pp. 833–851. Springer, Cham (2018). https://doi.org/10.1007/978-3-030-01234-2_49
18. Louche, A., Maurel, M., Simonnot, G., Peri, G., Iqbal, M.: Determination of Angstrom's turbidity coefficient from direct total solar irradiance measurements. *Sol. Energy* **38**(2), 89–96 (1987)
19. Woolley, H.: *Urban Open Spaces*. Taylor and Francis, Abingdon (2003)
20. 黄卓迪. 城市街道绿化对室外热舒适的影响研究. 华中农业大. (in Chinese)
21. Sarkar, C., Webster, C., Gallacher, J.: *Healthy Cities—Public Health Through Urban Planning*. Edward Elgar, Cheltenham (2014)
22. Takano, T., Nakamura, K., Watanabe, M.: Urban residential environments and senior citizens' longevity in megacity areas: the importance of walkable green spaces. *J. Epidemiol. Commun. Health* **56**(12), 913–918 (2002). <https://doi.org/10.1136/jech.56.12.913>
23. Maas, J., Van Dillen, S.M.E., Verheij, R.A., et al.: Social contacts as a possible mechanism behind the relation between green space and health. *Health Place* **15**(2), 586–595 (2009)
24. Bricker, K.S., Hendricks, W.W., Greenwood, J.B., Aschenbrenner, C.A.: Californians' perceptions of the influence of parks and recreation on quality of life. *J. Park Recreat. Adm.* **34**(3), 64–82 (2016). <https://doi.org/10.18666/JPRA-2016-V34-I3-7441>
25. Ekkel, E.D., de Vries, S.: Nearby green space and human health: evaluating accessibility metrics. *Landsc. Urban Plan.* **157**, 214–220 (2017)
26. Xu, K., Tartakovsky, A.M., Burghardt, J., et al.: Learning viscoelasticity models from indirect data using deep neural networks. *Comput. Methods Appl. Mech. Eng.* **387**, 114124 (2021)
27. Climate Bulletin of Fujian Province in 2020. <https://weibo.com/ttarticle/p/show?id=2309404614706022449491>